Chinese Chemical Letters 37 (2026) 111337

Contents lists available at ScienceDirect

Chinese Chemical Letters

journal homepage: www.elsevier.com/locate/cclet

A BODIPY-based ratiometric fluorescent probe for imaging of Zn^{2+} in ferroptosis

Yaheng Li[a], Weijiang He[a,c], Yuncong Chen[a,b,c,*], Zijian Guo[a,c,*]

[a] State Key Laboratory of Coordination Chemistry, School of Chemistry and Chemical Engineering, Chemistry and Biomedicine Innovation Center (ChemBIC), ChemBioMed Interdisciplinary Research Center, Nanjing University, Nanjing 210023, China
[b] Department of Cardiothoracic Surgery, Nanjing Drum Tower Hospital, Medical School, Nanjing University, Nanjing 210008, China
[c] Nanchuang (Jiangsu) Institute of Chemistry and Health, Nanjing 210000, China

ARTICLE INFO

Article history:
Received 23 January 2025
Revised 14 May 2025
Accepted 16 May 2025
Available online 16 May 2025

Keywords:
Zn^{2+}
Ferroptosis
Fluorescence imaging
BODIPY
Ratiometric probe

ABSTRACT

Ferroptosis is a cell death pathway that plays a crucial role in numerous biological processes. Although closely related to ferrous ion, the execution of ferroptosis was found to be impacted by zinc ion (Zn^{2+}) in recent years. However, most of the related researches focused on the effects of exogenously added Zn^{2+}, while the fundamental understanding of endogenous Zn^{2+} during ferroptosis still needs further exploration. Herein, a ratiometric fluorescent probe based on pyridine-substituted boron dipyrromethene (BODIPY) fluorophore (BDP-p) was designed to track the endogenous Zn^{2+} in cells during ferroptosis process. Zn^{2+} coordination induced an enhancement on the intramolecular charge transfer (ICT), leading to an obvious red shift from 563 nm to 594 nm. In A549 cells, we found fluorescence ratio of the probe elevated in some discrete regions during erastin induced ferroptosis, and this change followed the same trend as the reactive oxygen species (ROS) level. The results suggested that the Zn^{2+} would be localized in some discrete areas in A549 cells during ferroptosis. This work not only provided a reliable design strategy for developing ratiometric probes of Zn^{2+}, but also supplemented the current understanding of the non-negligible role of Zn^{2+} in ferroptosis.

© 2026 Published by Elsevier B.V. on behalf of Chinese Chemical Society and Institute of Materia Medica, Chinese Academy of Medical Sciences.

Ferroptosis, a type of programmed cell death that is ferrous ion dependent and executed by lipid peroxidation, is closely associated with various pathological processes of animals and plants [1,2]. For human, ferroptosis involved in diseases like impairment and cancers in liver, brain, kidney and heart [3]. Some tumors are reported to be more fragile to ferroptosis inducers due to enhanced iron metabolism and higher dependency on cysteine and glutathione [4–6]. In this way, ferroptosis inducers are increasingly tried out by researchers to selectively eliminate cancer cells [7], especially those that are resistant to classical chemotherapy drugs [8]. Besides conventional inducers like erastin and methyl-(1*S*,3*R*)-2-(2-chloroacetyl)-1-(4-methoxycarbonylphenyl)-1,3,4,9-tetrahydropyrido[3,4-b]indole-3-carboxylate (RSL3), metal ions can also act as ferroptosis inducers by affecting varied cell pathways [9]. Recent years, the crosstalk between ferroptosis-related factors and zinc drew the interest of the researchers [10]. Exogenously added zinc salt was found to induce ferroptosis in A549 lung cancer cells analyzed by multi-omics method [11]. Furthermore, this promoting effect in the other two types of cancer cells (MDA-MB-231 and HT-1080) was also reported [12]. The added zinc ion enhances the phosphorylation of the x_c^- system, consequently inhibiting its activity. Additionally, it enhances the expression of ferroptosis-related proteins like transferrin receptor protein 1 (CD71), transferrin, and high mobility group box 1 protein (HMGB1), while significantly reducing the expression of glutathione peroxidase 4 (GPX4), ferritin, and solute carrier family 7 member 11 gene (SLC7A11) [11,13]. All of these alterations facilitate the occurrence of ferroptosis. Inhibition of ZIP7 (a Zn^{2+} transporter) could cause endoplasmic reticulum (ER) stress, which protected cells from erastin-induced ferroptosis, suggesting that the transportation of zinc by ZIP7 was a key factor in ferroptosis [12]. Nevertheless, zinc salt does not always sensitize cells to ferroptosis. For neuron cell VSC4.1, zinc ion supplementation can inhibit ferroptosis *via* nuclear factor erythroid 2-related factor 2/heme oxygenase 1 (NRF2/HO-1) pathway [14]. The reported zinc supplementation therapy usually requires a high dose with potential toxicity and shows huge difference in efficacy determined by cell types [12,15]. The exploration of the Zn^{2+} behavior in cells may help to resolve these problems.

Zinc can stabilize proteins and adjust their functions *via* coordination and is released from them during oxidative stress to form a

* Corresponding authors.
E-mail addresses: chenyc@nju.edu.cn (Y. Chen), zguo@nju.edu.cn (Z. Guo).

https://doi.org/10.1016/j.cclet.2025.111337
1001-8417/© 2026 Published by Elsevier B.V. on behalf of Chinese Chemical Society and Institute of Materia Medica, Chinese Academy of Medical Sciences.

negative feedback regulation [16]. In terms of oxidative stress, zinc ions can also coordinate with various biothiols in cells, mutually regulating their free concentrations. Cells directly utilize biothiols such as glutathione to scavenge oxidative species, and this process is also affected by the zinc ion-regulated activity of biothiol oxidase [17]. Excessive zinc ions can also displace iron in proteins for respiratory chain, thereby promoting oxidative stress [11,18]. The above-mentioned facts indicate that zinc may act as a messenger in ferroptosis with oxidative context. The specific role of zinc in cell death appears intrinsically linked to its subcellular localization. Tracing Zn^{2+} with imaging technology to disclose the relevant pathways can be beneficial to improve the effect of zinc therapy. However, there are few literatures to disclose the behavior of endogenous Zn^{2+} during ferroptosis with imaging method. A reliable zinc sensor is in high demand for the study of the relationship of endogenous Zn^{2+} and ferroptosis. Besides fluorescence imaging, the main detecting methods for biological Zn^{2+} are atomic spectroscopy, mass spectroscopy, magnetic resonance imaging and so on [19], but most of them cause damage to living sample more or less and cannot achieve flexible real-time imaging. Fluorescent probe has been adopting as a powerful tool for biological imaging [20], and organic small molecule probes possess the virtue of flexible design, low cost, convenient use, and non-invasiveness [21]. A variety of biomarkers have been traced using fluorescent probes during ferroptosis to assist in the study of the effects of these biomarkers [22,23], some of which have been reported to have close associations with zinc ion-related pathways [24–26]. Among fluorescent sensors, ratiometric ones usually are more attractive due to their potential for quantitative detection [27]. There are successful examples to devise organic small molecule Zn^{2+} probes [28,29]. Unfortunately, because the hetero-atoms of the uncoordinated chelators along with the mechanism of photo-induced electron transfer, only a small part of the present literatures for ratiometric Zn^{2+} probes present significantly separated fluorescence peaks [30,31]. Moreover, current limitations in zinc probe design, particularly the trade-off between sensitivity, selectivity, biocompatibility, and spectral properties, necessitate innovative sensor development for studying zinc biology in ferroptosis-related environments.

To address this need, we engineered a β-functionalized boron dipyrromethene (BODIPY)-based ratiometric probe through strategic heterocycle conjugation. The β-position aromatic rings modulate both the electron density of the BODIPY core and the conjugation range. Hence electron-withdrawing pyridine was selected to construct an intramolecular charge transfer (ICT) system, and the probe with electron-donating furan was set as a control (probes BDP-p and BDP-f, respectively, Fig. 1a). The heterocycle was bonded at the β-position to efficiently coordinate to the Zn^{2+} captured with the chelator N^1,N^1-bis(pyridin-2-ylmethyl) ethane-1,2-diamine (BPEA) at the α-position. BPEA ensured adequate affinity to Zn^{2+} and provided dissociable hydrogen atom during coordination, while its secondary amine protons participated in hydrogen bonding with the β-pyridine nitrogen. We found that the electron-withdrawing pyridine cycle endowed the probe BDP-p with a ratiometric response in fluorescence after chelating with Zn^{2+}. In contrast, its furan-substituted counterpart BDP-f showed almost no Zn^{2+} sensing capacity. Using BDP-p as the imaging agent, we found the free Zn^{2+} level elevated during ferroptosis induced by erastin.

Both probes were fully characterized using nuclear magnetic resonance (NMR) and mass spectrometry (Scheme S1 and Figs. S1-S24 in Supporting information). BDP-p showed as absorption peak at around 540 nm and an emission maximum at about 563 nm. Upon Zn^{2+} addition, a slight red-shifted and broadened absorption with a distinct emission red-shift (563 nm shifted to 594 nm, Figs. 1b and c) were observed. However, BDP-f showed a larger Stokes

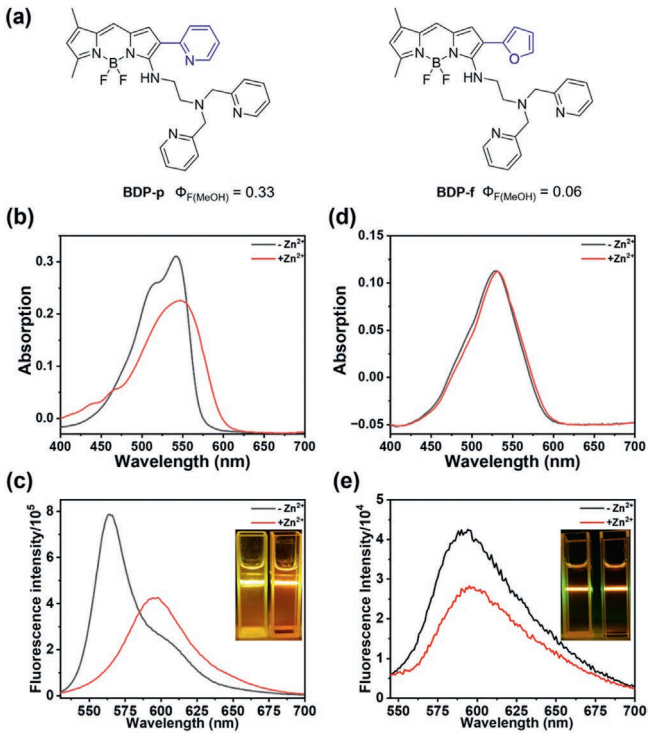


Fig. 1. The chemical structures of BDP-p and BDP-f (a). The absorption spectra of BDP-p (b) and BDP-f (d), and the fluorescence spectra of BDP-p (c) and BDP-f (e), tested in acetonitrile/2-[4-(2-hydroxyethyl)piperazin-1-yl]ethanesulfonic acid (HEPES) buffer (50 mmol/L, 100 mmol/L KCl, pH 7.4) = 1:1, slit = 1/1 nm. Inset of (c) and (e): the corresponding photos of the solutions excited by a green laser.

shift, with minimal absorption changes and slightly decreased fluorescence intensity in response to Zn^{2+} (Figs. 1d and e). Additionally, the fluorescence quantum yields (QYs) of BDP-f in methanol ($\Phi_F = 0.06$) was remarkably lower than that of BDP-p ($\Phi_F = 0.33$). The higher QY of BDP-p might be attributed to the smaller Stokes shift than that of BDP-f, which usually means smaller vibrational reorganization energy in the excited states. The results suggest that the β-pyridine group is essential for higher QY and ratiometric Zn^{2+} sensing.

To understand the mechanism of different spectroscopic and Zn^{2+} sensing properties of the two probes, the ^{1}H NMR Zn^{2+} titration and theoretical calculation were conducted (Fig. 2 and Fig. S25 in Supporting information). The chemical shift of proton H_1 in BDP-p was at 10.95 (Figs. 2a and b), whereas that of BDP-f was at 7.66 (Fig. 2c). This data suggested a strong intramolecular hydrogen bond formed in BDP-p. Moreover, β-pyridine protons in BDP-p (H_a-H_d, marked in blue) shifted downfield, while BODIPY core protons (H_2, H_4, marked in red) shifted upfield, indicating Zn^{2+} binding to the β-pyridine nitrogen and deprotonation of the -NH- group (Figs. 2a and b). The deprotonation of the -NH- group could significantly enhance the ICT effect of BDP-p, leading to the redshift on absorption and emission spectra. In contrast, for BDP-f, the signals of H_A-H_D possessed obvious shift to downfield while those of H_2 and H_4 on the BODIPY core hardly changed (marked in red), suggesting the distinct dipicolylamine coordination but weak coordination of the furan O atom (Fig. 2c). The calculated ground state conformations of the two probes also supported our speculation (Fig. S25). In the optimal ground-state conformation, the hydrogen bond between the secondary amine group and the adjacent heterocyclic ring in BDP-p (N-H···N distance: 1.7 Å) was shorter than that in BDP-f (N-H···O distance: 2.0 Å). The formation of the intramolecular hydrogen bond could enhance the rigidity of the BDP-p molecule, thereby inhibiting non-radiative transition and increasing its quan-

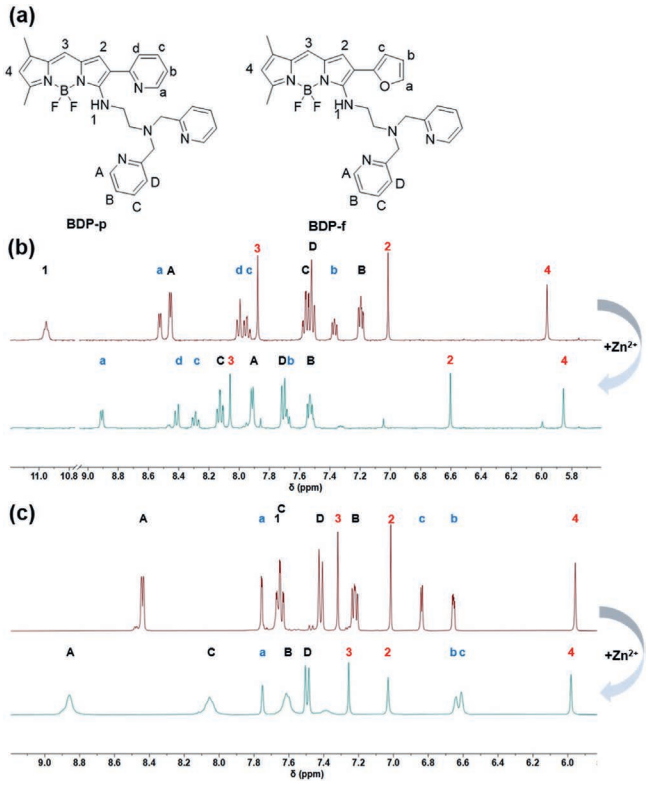


Fig. 2. (a) The number of each hydrogen presented in the following ^{1}H NMR spectra. (b) The ^{1}H NMR of the BDP-p before (up) and after (down) the addition of 1 equiv. of $ZnCl_2$. (c) The ^{1}H NMR of the BDP-f before (up) and after (down) the addition of 1 equiv. of $ZnCl_2$ (solvent: DMSO–d_6, 400 MHz).

tum yield. The results demonstrated that the β-pyridine modification not only help increasing the quantum yield of BDP-p by facilitating the intracellular H-bond formation, but also played an essential role in the Zn^{2+} coordination which leads to ratiometric sensing ability.

Next, we conducted the fluorescent Zn^{2+} titration of BDP-p (Fig. 3a). The dissociation constant K_d was calculated to be 2.5 nmol/L (Fig. S26 in Supporting information). Besides the high sensitivity, the coordination was also very rapid (Fig. 3b). The 1:1 Zn^{2+} binding stoichiometry was confirmed by Job's plot and mass spectrometry (Fig. 3c and Fig. S27 in Supporting information). The selectivity of BDP-p was also checked (Fig. 3d). The interference from most of the common metal ions and hydrogen peroxide was in an acceptable range. Although some ions indeed obviously impacted the ratio value of the fluorescence at one equivalent concentration, their concentrations were proved to be far lower than Zn^{2+} in biological environment [32–34], so that they would not interfere with the detection in cells. In this way, it could be preliminarily assumed that BDP-p was qualified to visualize the change of Zn^{2+} level in cells.

Encouraged by the solution-phase results, we next investigated BDP-p's capability to monitor both exogenous and endogenous free Zn^{2+} in live cells. As shown in Figs. 4a–j, zinc pyrithione was used to directly supplement free Zn^{2+} to cells, and a well-known biothiol scavenger *N*-ethylmaleimide (NEM) was used to liberate protein-bound zinc into the labile pool (Figs. 4k–o) [35]. In these two occasions, we found the fluorescence intensity in the green channel decreased and that of the red channel enhanced, yielding the elevated ratio of the two fluorescence channels. After the incubation of NEM, the labile zinc was sequestered by a high affinity Zn^{2+} chelator *N*,*N*,*N*′,*N*′-tetrakis-(2-pyridylmethyl) ethylenediamine (TPEN), and the ratio value dropped dramatically (Figs. 4p–u). Moreover, the cell viability assay confirmed the biocompati-

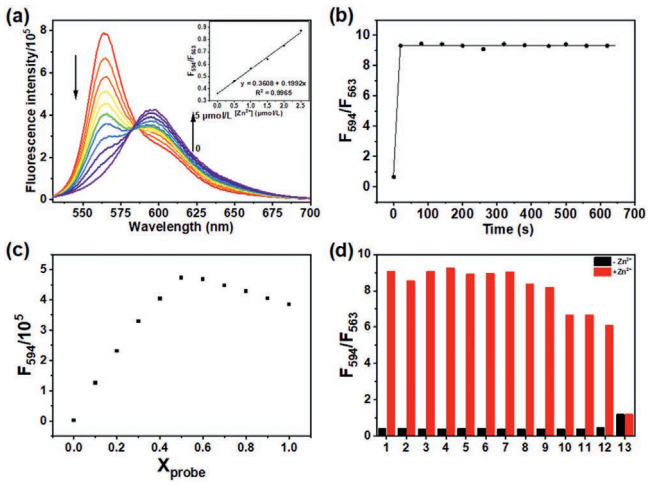


Fig. 3. The optical properties of BDP-p (5 μmol/L) tested in acetonitrile/HEPES buffer (50 mmol/L, 100 mmol/L KCl, pH 7.4) = 1:1, slit = 1/1 nm. (a) The fluorescence spectra of BDP-p titrated by $ZnCl_2$ solution, inset: the linear fitting curve within the 0.5 equiv. titration. (b) The ratio of fluorescence intensities at 594 and 563 nm against time. (c) The Job's plot of BDP-p, $X_{probe} = c_{probe}/(c_{probe} + [Zn^{2+}])$. (d) The fluorescence ratio (594 nm/563 nm) of BDP-p mixed with varied metal ions at the presence of three equivalents of Zn^{2+} (red) or not (black). 1. Blank; 2. Fe^{2+}; 3. H_2O_2; 4. Mn^{2+}; 5. 0.1 equiv. Co^{2+}; 6. 0.1 equiv. Ni^{2+}; 7. 0.001 equiv. Cu^{2+}; 8. 100 equiv. Na^+ + 100 equiv. K^+ + 40 equiv. Ca^{2+} + 40 equiv. Mg^{2+}; 9. Fe^{3+}; 10. Hg^{2+}; 11. Pb^{2+}; 12. Cd^{2+} 13. Cu^{2+}, the metal ions were 1 equiv. unless specified.

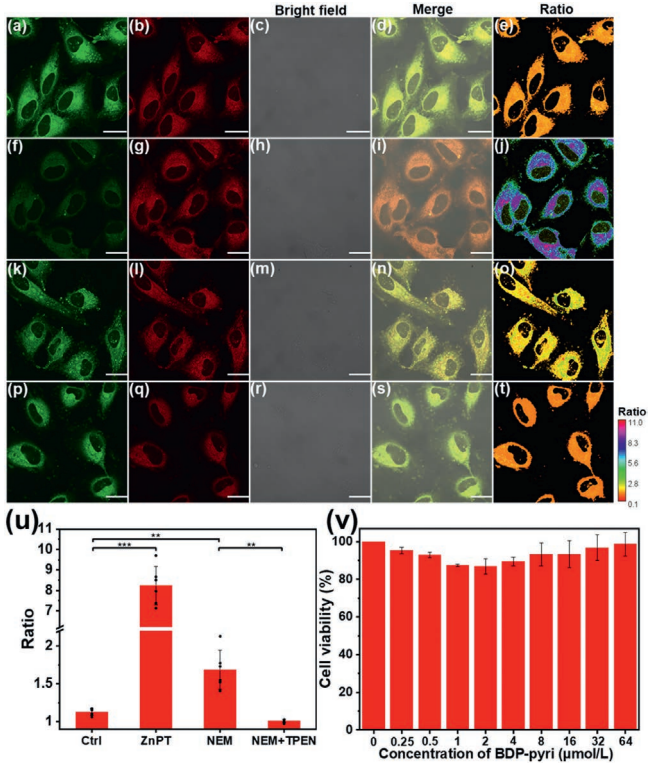


Fig. 4. Images of A549 cells incubated with 2 μmol/L of BDP-p for 1 h and then treated with the following: (a–e) culture medium (control); (f–j) 10 μmol/L of zinc pyrithione (ZnPT), incubated for 20 min; (k–o) 50 μmol/L of NEM incubated for 20 min; (p–t) 50 μmol/L of NEM incubated for 20 min, and then cells were treated with 50 μmol/L of TPEN for 15 min. Green channel: 555–585 nm, red channel: 598–628 nm. Both of the channels were excited at 543 nm. Scale bar: 20 μm. (u) The calculation results of the ratio value in each experiment group, ratio = red channel/green channel. (v) Cell viability *versus* the concentration of BDP-p in methylthiazolyldiphenyl-tetrazolium bromide (MTT) assay, the cells were incubated with BDP-p for 12 h. Data are presented as mean ± standard deviation ($n = 6$ for u and $n = 3$ for v). The significance comparison of differences between groups was conducted using a two-tailed *t*-test. $^{**}P < 0.01$, $^{***}P < 0.001$.

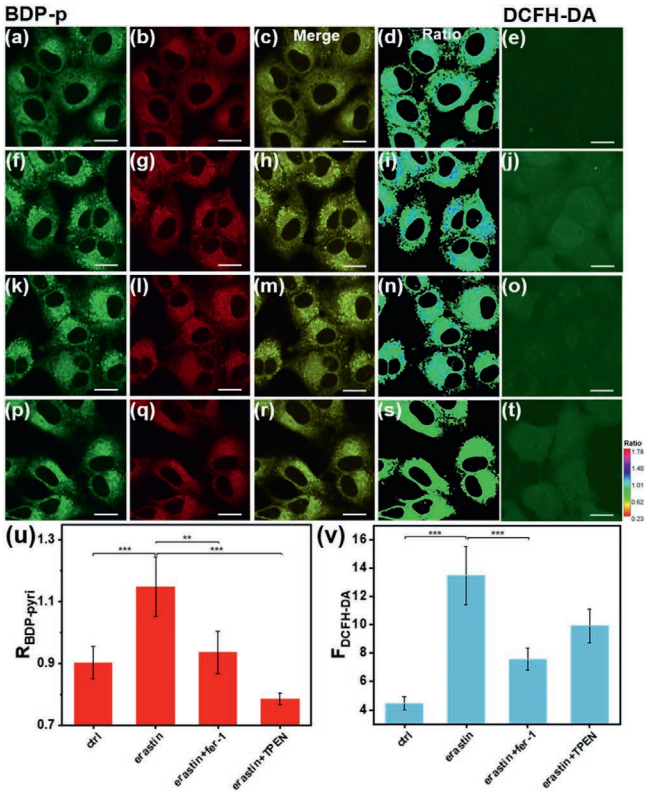


Fig. 5. Images of A549 cells treated with following species for 24 h and then incubated with 2 μmol/L of BDP-p for 1 h or 10 μmol/L of DCFH-DA for 0.5 h: (a–e) blank; (f–j) 10 μmol/L of erastin; (k–o) 10 μmol/L of erastin and 5 μmol/L of fer-1; (p–t) 10 μmol/L of erastin for 24 h and 40 μmol/L of TPEN for 20 min. Scale bar: 20 μm. (u) The ratio value of BDP-p (R_{BDP-p}) in each experiment group, ratio = red channel/green channel. Green channel: 555–585 nm, red channel: 598–628 nm. Both of the channels were excited at 543 nm. (v) The fluorescence intensity of DCFH-DA ($F_{DCFH-DA}$) in each experiment group. The ROS levels were determined by DCFH-DA probe. Data are presented as mean ± standard deviation ($n = 6$). The significance comparison of differences between groups was conducted using a two-tailed *t*-test. $^{**}P < 0.01$, $^{***}P < 0.001$.

bility of BDP-p in its imaging concentration (Fig. 4v and Fig. S28 in Supporting information). The colocalization experiments showed no organelle-specific accumulation of BDP-p (Fig. S29 in Supporting information).

Finally, the fluctuation of the free Zn^{2+} level during ferroptosis process was imaged by BDP-p (Figs. 5a–d, f–i, k–n). Erastin had been well acknowledged to induce ferroptosis in A549 cells with specified time and concentration [36,37]. The images indicated that there were some discrete zones appeared in which the Zn^{2+} level elevated, as represented by fluorescence ratio enhancement (Fig. 5i). Meanwhile, an increased level of reactive oxygen species (ROS) was also observed by 2,7-dichlorodihydrofluorescein diacetate (DCFH-DA) (Figs. 5e and j). When ferroptosis was inhibited by ferrostatin-1 (fer-1), the zinc elevation was suppressed consequently, concomitant with a suppressed ROS level (Figs. 5j, o, u and v). Notably, TPEN treatment leads to a ratio decrease, suggesting that the observed ratio increase during ferroptosis was caused by enhanced free Zn^{2+} (Figs. 5p–u). The results indicated that the elevated ROS during ferroptosis might lead to free Zn^{2+} release. To underscore ratiometric advantage of BDP-p, we performed parallel experiments with an intensity-based commercial probe Zinpyr-1 (Fig. S30 in Supporting information). While both probes detected erastin-induced Zn^{2+} increases, Zinpyr-1 exhibited probe aggregation artifacts, evidenced by the obscured true Zn^{2+} distribution. Therefore, BDP-p was capable to visualize the intracellular microzones where free Zn^{2+} elevated during ferroptosis.

In summary, we designed a ratiometric Zn^{2+} probe by introducing a pyridyl group at the *ortho*-position of the chelating group linked to BODIPY fluorophore. After chelating with Zn^{2+}, BDP-p exhibited enhanced ICT effect due to the stronger electron donating ability of deprotonated -NH- group and stronger electron-withdrawing ability of β-pyridine, leading to an emission band redshift from 563 nm to 594 nm. Using this probe, we found that Zn^{2+} accumulated in some discrete regions in A549 cells during ferroptosis induced by erastin. This work may be helpful to the understanding of how the endogenous Zn^{2+} plays its role in ferroptosis. Our next efforts will be devoted to further investigate the fluctuating Zn^{2+} level during ferroptosis in organelle level.

Declaration of competing interest

The authors declare that they have no known competing financial interests or personal relationships that could have appeared to influence the work reported in this paper.

CRediT authorship contribution statement

Yaheng Li: Writing – original draft, Methodology, Investigation, Data curation, Conceptualization. **Weijiang He:** Writing – original draft, Funding acquisition. **Yuncong Chen:** Writing – review & editing, Supervision, Project administration, Funding acquisition, Conceptualization. **Zijian Guo:** Writing – review & editing, Supervision, Project administration, Funding acquisition, Conceptualization.

Acknowledgments

We acknowledge funds from the Natural Science Foundation of China (Nos. 22293050, 22293051, 92153303, 22477054, 22377050), the Natural Science Foundation of Jiangsu Province (No. BK20232020), and the Excellent Research Program of Nanjing University (No. ZYJH004).

Supplementary materials

Supplementary material associated with this article can be found, in the online version, at doi:10.1016/j.cclet.2025.111337.

References

[1] B.R. Stockwell, X. Jiang, W. Gu, Trends Cell Biol. 30 (2020) 478–490.
[2] A.M. Distéfano, G.A. López, N. Setzes, et al., J. Exp. Bot. 72 (2020) 2125–2135.
[3] Z. Li, L. Chen, C. Chen, et al., Biomark. Res. 8 (2020) 58.
[4] C.M. Bebber, F. Müller, L.Prieto Clemente, et al., Cancers 12 (2020) 164.
[5] M. Jiang, M. Qiao, C. Zhao, et al., Transl. Lung Cancer Res. 9 (2020) 1569–1584.
[6] K.D. Tousignant, A. Rockstroh, B.L.J. Poad, et al., Cancer Metab. 8 (2020) 11.
[7] C. Liang, X. Zhang, M. Yang, et al., Adv. Mater. 31 (2019) e1904197.
[8] M. Sato, R. Kusumi, S. Hamashima, et al., Sci. Rep. 8 (2018) 968.
[9] K. Sahoo, A. Sharma, Apoptosis 28 (2023) 277–292.
[10] K. Ke, L. Li, C. Lu, et al., Front. Oncol. 12 (2022) 916082.
[11] L.D. Palmer, A.T. Jordan, K.N. Maloney, et al., Metallomics 11 (2019) 982–993.
[12] P.H. Chen, J. Wu, Y. Xu, et al., Cell Death Dis. 12 (2021) 198.
[13] Q. Li, Q. Yang, P. Guo, et al., Food Chem. Toxicol. 179 (2023) 113950.
[14] M.H. Ge, H. Tian, L. Mao, et al., CNS Neurosci. Ther. 27 (2021) 1023–1040.
[15] J. Zou, L. Wang, H. Tang, et al., Int. J. Mol. Sci. 22 (2021) 13335.
[16] P.J. Little, R. Bhattacharya, A.E. Moreyra, et al., Nutrition 26 (2010) 1050–1057.
[17] U.I. Walther, B. Wilhelm, S. Walther, et al., Biol. Trace Elem. Res. 78 (2000) 163–177.
[18] E. Rudolf, Acta Med. 50 (2007) 43–49.
[19] R. Lobinski, C. Moulin, R. Ortega, Biochimie 88 (2006) 1591–1604.
[20] M. Sitara, W. Zhang, H. Gao, et al., Chem. Biomed. Imaging 2 (2024) 526–541.
[21] D. Seah, Z. Cheng, M. Vendrell, ACS Nano 17 (2023) 19478–19490.
[22] J. Zeng, M. Liu, T. Yang, et al., Chin. Chem. Lett. 36 (2025) 110166.
[23] X. Tian, D. Wu, W. Wei, et al., Chin. Chem. Lett. 35 (2024) 108912.
[24] X. Tian, J. Cheng, L. Yang, et al., Chem. Biomed. Imaging 2 (2024) 518–525.
[25] R. He, D. Tang, N. Xu, et al., Chin. Chem. Lett. 35 (2024) 108658.
[26] H. Zhang, R. Feng, W. Yu, et al., Chin. Chem. Lett. 36 (2025) 110528.
[27] R. Gui, H. Jin, X. Bu, et al., Coord. Chem. Rev. 383 (2019) 82–103.
[28] Y. Chen, Molecules 29 (2024) 2542.

[29] J. Wang, Y. Li, Y. Pang, Chem. Biomed. Imaging 1 (2023) 537–540.
[30] S. Xia, J. Shen, J. Wang, et al., Sens. Actuators B: Chem. 258 (2018) 1279–1286.
[31] Z. Guo, G.H. Kim, I. Shin, et al., Biomaterials 33 (2012) 7818–7827.
[32] T.D. Rae, P.J. Schmidt, R.A. Pufahl, et al., Science 284 (1999) 805–808.
[33] Q. Pasha, S. Malik, M. Shah, J. Hazard. Mater. 153 (2008) 1215–1221.
[34] M. Yaman, Curr. Med. Chem. 13 (2006) 2513–2525.
[35] V.Q. Do, Y.S. Seo, J.M. Park, et al., Arch. Toxicol. 95 (2021) 541–556.
[36] S.W. Alvarez, V.O. Sviderskiy, E.M. Terzi, et al., Nature 551 (2017) 639–643.
[37] C. Huang, M. Yang, J. Deng, et al., Oncol. Rep. 40 (2018) 2363–2370.